NTATION PAGE

Form Approved
OBM No. 0704-0188

verage 1 hour per response, including the time for reviewing instructions, searching existing data sources, gathering and information. Send comments regarding this burden or any other aspect of this collection of information, including suggestions te for Information Operations and Reports, 1215 Jefferson Davis Highway, Suite 1204, Arlington, VA 22202-4302, and to 04-0188), Washington, DC 20503.

gency Use Only (Leave blank).	2. Report Date. March 1993	3. Report Type and Dates Covered. Final - Journal Article

itle and Subtitle.
assive Microwave Signatures of Fractures and Ridges in Sea Ice at 33.6 GHz /ertical Polarization) as Observed in Aircraft Images

5. Funding Numbers.
Program Element No. 0601153N
Project No. 3205
Task No. 050
Accession No. DN256025
Work Unit No. 13321D

uthor(s).
. Dennis Farmer, Duane T. Eppler, and Alan Lohanick*

erforming Organization Name(s) and Address(es).
aval Research Laboratory
ceanography Division
tennis Space Center, MS 39529-5004

8. Performing Organization Report Number.
JA 332:029:92

ponsoring/Monitoring Agency Name(s) and Address(es).
laval Research Laboratory
lasic Research Management Office
tennis Space Center, MS 39529-5004

10. Sponsoring/Monitoring Agency Report Number.
JA 332:029:92

DTIC ELECTE AUG 11 1993 S A D

Supplementary Notes.
ublished in Journal of Geophysical Research.

. Distribution/Availability Statement.
pproved for public release; distribution is unlimited.

12b. Distribution Code.

Abstract *(Maximum 200 words).*

An aircraft data set of coincident K_a band (33 GHz, vertical polarization) passive microwave images and aerial photographs cquired in the Chukchi-Beaufort Sea region in March 1983 was analyzed to evaluate radiometric signatures of deformational eatures that occur in sea ice. A total of 115 fractures and 197 pressure ridges were examined with respect to physical appearance relative age, snow cover, ice type, width, orientation) as observed in photographs, and radiometric character (brightness emperature, radiometric contrast with respect to adjacent ice, radiometric profile across the feature) as measured from digital assive microwave images. Of the deformational features that were observed in aerial photographs, 82% had radiometric ignatures of sufficient contrast to be observed in passive microwave images. Fractures and ridges have equal chance of letection, but fractures cannot be distinguished from pressure ridges on the basis of brightness temperature, radiometric contrast, r characteristics of radiometric profiles measured across these features.

Subject Terms.
ea ice classification, passive microwave, remote sensing

15. Number of Pages. 19

16. Price Code.

Security Classification of Report.	18. Security Classification of This Page.	19. Security Classification of Abstract.	20. Limitation of Abstract.
Unclassified	Unclassified	Unclassified	SAR

N 7540-01-280-5500

Standard Form 298 (Rev. 2-89)
Prescribed by ANSI Std. Z39-18
298-102

DISCLAIMER NOTICE

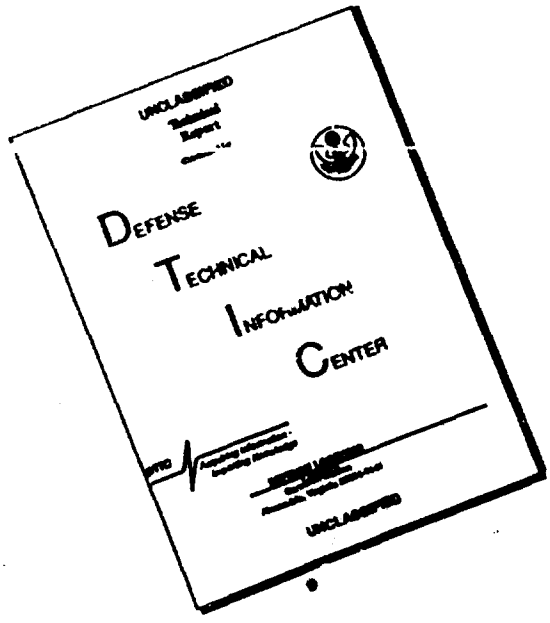

THIS DOCUMENT IS BEST QUALITY AVAILABLE. THE COPY FURNISHED TO DTIC CONTAINED A SIGNIFICANT NUMBER OF PAGES WHICH DO NOT REPRODUCE LEGIBLY.

DISCLAIMER NOTICE

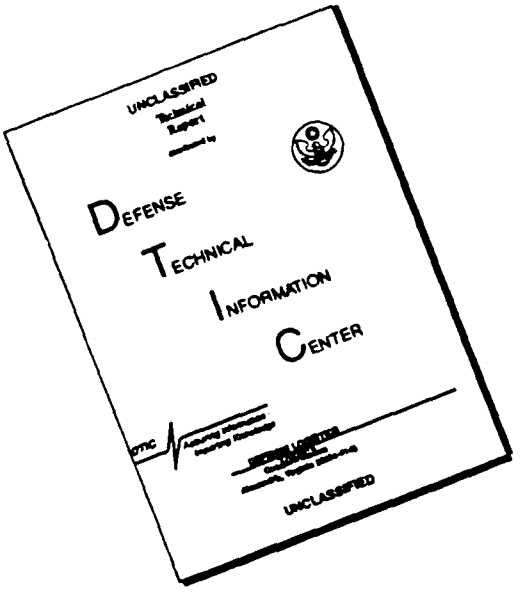

THIS DOCUMENT IS BEST QUALITY AVAILABLE. THE COPY FURNISHED TO DTIC CONTAINED A SIGNIFICANT NUMBER OF PAGES WHICH DO NOT REPRODUCE LEGIBLY.

JOURNAL OF GEOPHYSICAL RESEARCH, VOL. 98, NO. C3, PAGES 4645–4665, MARCH 15, 1993

Passive Microwave Signatures of Fractures and Ridges in Sea Ice at 33.6 GHz (Vertical Polarization) as Observed in Aircraft Images

L. DENNIS FARMER,[1] DUANE T. EPPLER,[1] AND ALAN W. LOHANICK[2]

Polar Oceanography Branch Office, Naval Research Laboratory, Hanover, New Hampshire

An aircraft data set of coincident K_a band (33.6 GHz, vertical polarization) passive microwave images and aerial photographs acquired in the Chukchi-Beaufort Sea region in March 1983 was analyzed to evaluate radiometric signatures of deformational features that occur in sea ice. A total of 115 fractures and 197 pressure ridges were examined with respect to physical appearance (relative age, snow cover, ice type, width, orientation) as observed in photographs, and radiometric character (brightness temperature, radiometric contrast with respect to adjacent ice, radiometric profile across the feature) as measured from digital passive microwave images. Of the deformational features that were observed in aerial photographs, 82% had radiometric signatures of sufficient contrast to be observed in passive microwave images. Fractures and ridges have equal chance of detection, but fractures cannot be distinguished from pressure ridges on the basis of brightness temperature, radiometric contrast, or characteristics of radiometric profiles measured across these features. However, visual analysis of passive microwave images, which takes into account contextual information, does allow fractures to be distinguished from pressure ridges in many instances. Radiometric signatures of both fractures and ridges are more likely to be radiometrically warmer (as opposed to cooler) than adjacent ice, which suggests that saline ice is a significant constituent of most deformational features. New ridges are more likely to be radiometrically warm than old ridges, probably because brine drains from the ridge as it ages (which reduces emissivity) and snow accumulates in drifts along the ridge trend (which enhances scattering). However, brightness temperatures of snow-covered ridges extend across a range that is approximately 15 K cooler, and 10 K warmer than the range observed for snow-free ridges. Old features show higher radiometric contrast with respect to adjacent ice than new features, which increases their probability of detection.

1. INTRODUCTION

Technical and operational applications require accurate detection and characterization of deformational features, such as fractures and ridges, that occur in the arctic sea ice pack. Information concerning the frequency of occurrence, spacing, width, length, and orientation of fractures, leads, and pressure ridges is required by global climate models and by dynamic-thermodynamic sea ice models that predict ice motion, growth, and decay. Similar information is needed for operational applications that involve ship navigation, icebreaker support, offshore oil exploration, and air cushion vehicle routing. The hostile arctic environment, which is characterized by long dark periods, frequent cloud cover, and vast uninhabited areas, dictates that data in support of these requirements be obtained from sensors carried aboard aircraft or satellites.

Microwave imagers represent candidate sensors for these tasks because they provide high-quality images of surface features in spite of darkness and cloud cover. Neither active nor passive microwave sensors have been evaluated rigorously with respect to their ability to map deformational features in sea ice. Past work in evaluating operational resolution of passive microwave sensors, the class of sensors with which work reported below is concerned, has been directed primarily toward defining radiometric resolution rather than spatial resolution [cf. *Hollinger et al.*, 1990]. Most such work was intended to provide average radiometric characteristics of different sea ice types for verifying satellite sensors of low spatial resolution [*Wilheit et al.*, 1972; *Gloersen et al.*, 1973, 1978; *Campbell et al.*, 1976, 1978; *Troy et al.*, 1981; *Cavalieri et al.*, 1991]. More recent

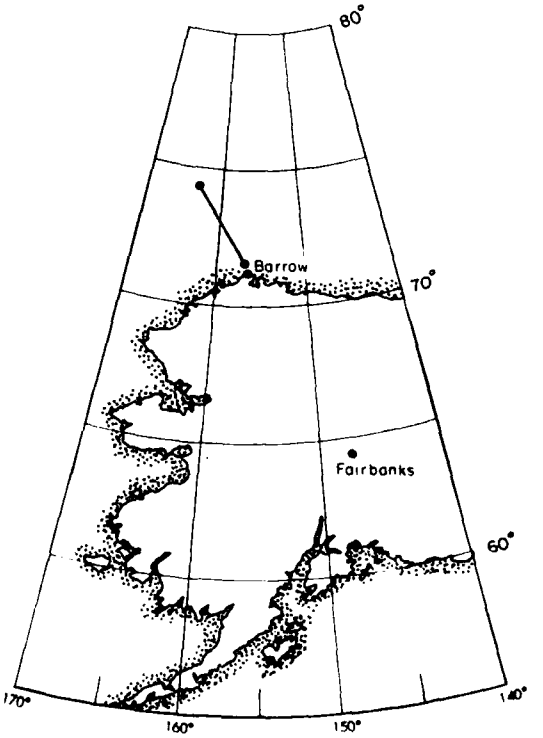

Fig. 1. Location map showing flight track along which data used here were collected on March 20, 1983.

[1]Now at Bronson Hills Associates, Fairlee, Vermont.
[2]Now at AWL Research, Lebanon, New Hampshire.

Paper number 92JC02753.

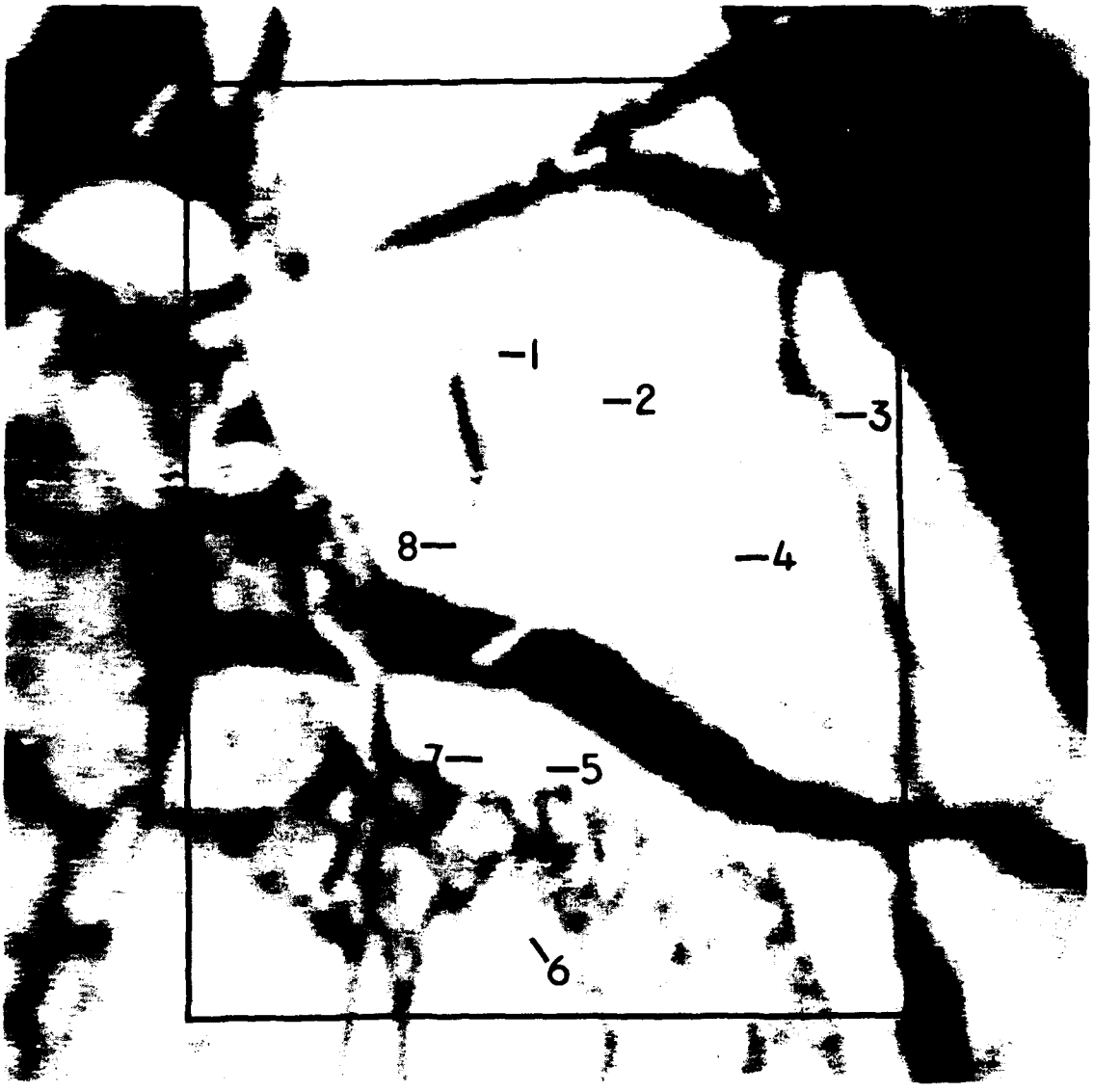

Fig. 2*a*

Fig. 2. Example of data used to derive statistics on ridge and fracture signatures. (*a*) Coincident passive microwave image showing the same features indicated on the photograph in Figure 2*b*. The box indicates the area covered by the photograph. Radiometrically cool old ice floes are shown in light tones; dark tones correspond to radiometrically warm first-year ice. (*b*) Aerial photograph that shows an area approximately 2300 m square. Numbers point to features that are described in Table 1. Boxes around features 2 and 5, which are narrow cracks, indicate area enlarged in Figures 6*a* and 6*b*.

work investigated radiometric variability observed at smaller scales [*Ketchum and Lohanick*, 1980; *Eppler et al.*, 1986; *Eppler and Farmer*, 1991], in some cases at meter scales [*Lohanick*, 1982; *Grenfell and Lohanick*, 1985; *Lohanick and Grenfell*, 1986], to support radiometric interpretation of images obtained with higher resolution airborne sensors. These more recent studies bring local radiometric variability typical of sea ice into better focus but fall short of defining passive microwave signatures associated with specific deformational features that occur in sea ice, such as fractures and ridges.

Characteristics of deformational features that determine their radiometric signature and influence their detection remain poorly understood. We know, for example, that ridges within a floe of old ice broaden the range of brightness temperatures associated with the floe [*Eppler et al.*, 1986; *Livingstone et al.*, 1987]. It is not clear, however, why some ridges appear as radiometrically cool features, some as radiometrically warm features, and some go unobserved, not only in passive microwave images [*Eppler et al.*, 1986], but in active microwave images as well [*Ketchum and Lohanick*, 1980; *Leppäranta and Thompson*, 1989].

Most deformational features that occur in sea ice are manifest in remotely sensed imagery as series of linear features. In this paper we address issues that concern detection and interpretation of these lineaments in K_a band (33.6 GHz, vertical polarization (V-pol)) passive microwave imagery. (All imagery used in this analysis was obtained at 33.6 GHz, vertical polarization. Radiometric signatures of deformational features at other frequencies and polarizations

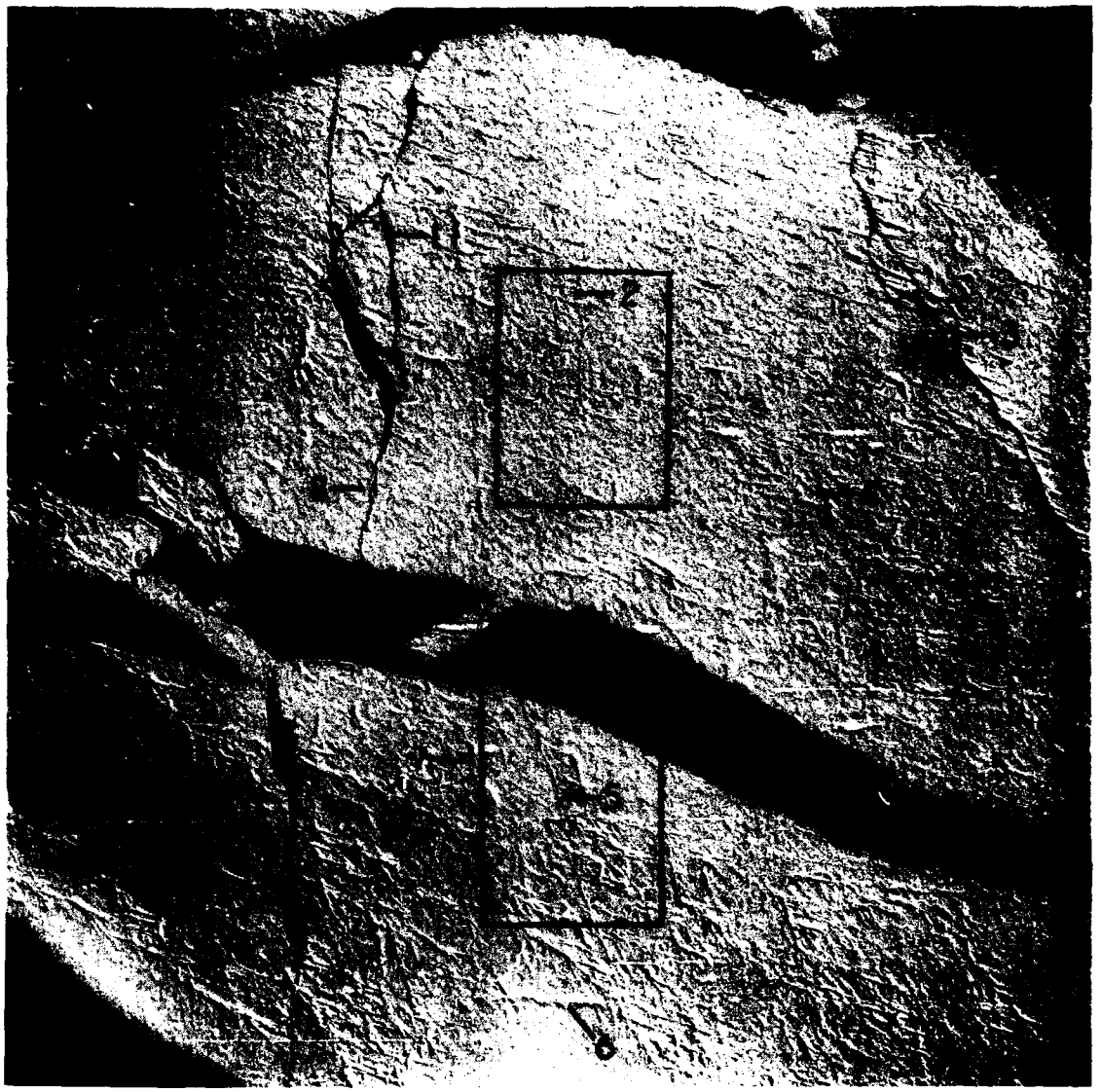

Fig. 2*b*

may differ from those presented here.) Specifically, we evaluate the likelihood of observing deformational features in K_a band passive microwave imagery and assess the separability of ridge signatures from fracture signatures. We use a data set of aircraft passive microwave images and coincident fine-resolution aerial photographs that show sea ice conditions in the Chukchi-Beaufort Sea region north of Barrow, Alaska, to analyze factors and conditions that mediate feature signatures and that enhance or degrade the probability of detection. On the basis of these observations and prevailing microwave theory, we develop conceptual radiometric models that describe phenomena from which signatures of deformational features observed in passive microwave images arise.

2. Description of Data and Surface Conditions

Data used for this study include aircraft digital passive microwave images obtained with the Navy K_a band (33.6 GHz, V-pol) Radiometric Mapping System (KRMS) and coincident high-resolution black-and-white aerial photographs obtained with a Wild RC-10 camera. These data were collected in the Beaufort-Chukchi Sea region on March 20, 1983, from a flight altitude of 1500 m. Both sensors were carried aboard the same aircraft. These data provide a continuous record of ice conditions measured at visible and microwave frequencies along a straight-line track 320 km in length that extends north-northwestward from a point approximately 30 km offshore from Barrow, Alaska (Figure 1). Salient characteristics of the sensors are summarized below. *Eppler et al.* [1986] and *Eppler and Heydlauff* [1990] provide additional information concerning instrument characteristics and acquisition and processing of the data set.

2.1. *Passive Microwave Imagery*

Passive microwave imagery was obtained with the KRMS instrument. Data initially were recorded in analog form on tape. Subsequently, the data were digitized and recorded on 9-track tape using methods of *Eppler and Heydlauff* [1990]. Analysis was performed both manually using hard copy prints made from these digital tapes (Figure 2*a*) and digitally

TABLE 1. Example of Data Matrix Generated in First Phase of Data Analysis, Keyed to Features Identified in Figure 2

ID	Feature Type	Relative Age	Snow	Ice Type*	Orientation	Width, M	Relative Contrast†	Comment
1	fracture	new	no	gr>my	90	12	m-w	ice covered fracture
2	fracture	new	no	?>my	90	1.5	l-w	very narrow crack
3	ridge	old	yes	?>my	60	8	h-w	old ridge, drifted snow
4	?	old	yes	?>my	55	?	m-c	no indication of feature in microwave image
5	fracture	new	no	?>my	75	3	l-w	narrow crack, possibly with ridge
6	ridge	old	yes	?>my	0	11	h-c	old weathered ridge
7	ridge	old	yes	?>my	60	15	l-w	hummock
8	ridge/fracture	new	no	gr>my	90	15	m-w	new ridge and fracture combined

*Ice types are gr, gray ice, and my, multiyear ice.
†Abbreviations are l, low contrast; m, medium contrast; h, high contrast; w, warm feature; and c, cool feature.

using standard image processing software and display hardware. Gray values in some images were stretched linearly to maximize contrast. Aside from contrast enhancement, the images were not manipulated; filters were not applied to remove noise, sharpen edges, accentuate linear features, or enhance general image quality. Results presented here thus represent conservative estimates of the resolving capability of aircraft passive microwave sensors, inasmuch as the analysis is based on analysis of raw, unenhanced imagery.

KRMS operates at a center frequency of 33.6 GHz and senses vertically polarized radiation emanating from the Earth's surface. Sensitivity of the KRMS sensor as measured in bench tests is 0.05 K/s. Operational sensitivity is believed to be better than 0.5 K. Field of view is 100° centered at nadir, and the instantaneous 3-dB beam spot of the KRMS antenna is 1.0°. From the 1500-m flight altitude, the sensor paints a swath that is approximately 3.6 km across, which is somewhat broader than the 2.3-km swath of the aerial camera. The beam spot subtends a footprint from this flight altitude that is 26 m in diameter at nadir. Analog data recorded continuously across the 100° swath are digitized into image lines consisting of 512 pixels. Each pixel in a digital KRMS image thus represents a ground area that is approximately 5 m square.

Data used here were calibrated using the method of *Farmer et al.* [1990]. Tie points for the warm end of the spectrum are derived from a hot load embedded within the sensor. Cool tie points are derived from external targets imaged by the sensor, primarily ice-free ocean exposed in leads and polynyas. Brightness temperatures derived from digital radiances using this method are not calibrated values in a strict sense, since the cool tie point is not known absolutely. The conversion also assumes that there is no atmosphere between the sensor and the surface. Use of KRMS data in conjunction with data from other microwave sensors suggests, however, that error incurred using this method is not significant [*Cavalieri et al.*, 1991; *Eppler et al.*, 1992].

2.2. *Aerial Photography*

The Wild RC-10 aerial camera produces high-quality negatives on $9\frac{1}{2}$-inch-wide film (Figure 2*b*). Spatial resolution of the camera-lens-film system used from the 1500-m altitude that was flown is estimated at approximately 0.25 m, which is 2 orders of magnitude better than the 26-m resolution of the passive microwave sensor (compare Figures 2*a* and 2*b*). Analysis of the photographic data was performed using both original negatives and contact prints. Swath width of photo coverage is approximately 2.3 km centered both at aircraft nadir and within the KRMS swath. Ground area covered in adjacent photographs overlaps by approximately 60% so that features of interest can be viewed stereographically. Stereographic coverage coupled with fine resolution proved valuable in locating low-relief, indistinct features that produced distinct brightness temperature signatures in the passive microwave images.

2.3. *Meteorology*

Weather conditions were exceptional for the duration of the flight. The flight was made during midday; the sun was approximately 18° above the horizon at noon. The sky was cloud-free at all altitudes throughout the mission and haze was negligible, which permitted acquisition of black-and-white photographs of exceptionally high quality that show pressure ridges and fractures in excellent detail (Figure 2*b*). Surface parties camped on the ice near the southern terminus of the flight track reported cold (−10°C), dry conditions throughout the day. Surface observations showed that snow moisture was negligible and was insufficient to modulate microwave signatures.

2.4. *Sea Ice Conditions*

The area studied is located within the southern portion of the multiyear pack. Sea ice consists primarily of mixtures of multiyear ice and first-year ice, with multiyear ice dominant in most scenes; first-year ice typically fills leads between multiyear floes. Thin ice and open water form minor constituents of the pack and are associated mainly with two open leads observed near the southern terminus of the flight track. Ridges and fractures are present throughout the data set and occur in both multiyear ice and first-year ice. Visual analysis of the photographs suggests that the number of ridges and fractures observed within a given scene is relatively constant throughout the data set. The extent to which ice is deformed is typical of general conditions observed at other points in the multiyear pack. Indications of extreme deformation (exceptionally rugged ice surfaces, extensive rubble fields, highly fractured floes, abnormally high ridges) are not in evidence.

3. METHOD OF ANALYSIS

Analysis of the data was accomplished in two phases. During the first phase, aerial photographs were examined to

TABLE 2. Summary of Detection Frequency in Passive Microwave Images for Deformational Features Observed in Aerial Photographs

	Number Measured*	Number Resolved†	Percent Resolved†
All Fractures	115	95	82.6
New fractures	35	26	74.3
Old fractures	80	69	86.3
All Ridges	197	161	81.7
New ridges	61	43	70.5
Old ridges	136	118	86.7
All Features	312	256	82.0

*In photographs.
†In KRMS data.

TABLE 4. Relative Radiometric Contrast Between Deformational Features and Adjacent Ice

	Number of Features Sampled	Percent of Features With High Contrast	Percent of Features With Low Contrast	Percent of Features With No Contrast
All Fractures	115	56.5	26.1	17.4
New fractures	35	20.0	54.3	25.7
Old fractures	80	72.5	13.8	13.7
All Ridges	197	56.9	24.8	18.3
New ridges	61	44.3	26.2	29.5
Old ridges	136	62.4	24.3	13.3
All Features	312	56.7	25.3	18.0
New features	96	35.4	36.5	28.1
Old features	216	66.1	20.4	13.5

compile a sample of linear features (pressure ridges and fractures). Three hundred and twelve features were selected to represent the range of variability observed among ridges and fractures. Each of these features was described in terms of its type (pressure ridge or fracture), width, type of ice both within the feature and adjacent to the feature, presence or absence of snow, orientation of the feature trend with respect to KRMS scan direction, and relative age of the feature based on the freshness of its appearance in the photograph (the extent to which drifted snow is present and, in the case of ridges, whether individual blocks can be observed). In subsequent discussion, we refer to features that appear fresh and newly formed as new features, and those that appear weathered as old features. When this initial feature inventory was completed using photographs, an attempt was made to locate each of the 312 features on hard copy prints of the coincident KRMS images.

Figure 2 shows an example of a photograph with its coincident KRMS image. Features that were analyzed are identified by numbers on both images. Table 1 is the tabulated data matrix derived from the image pair in Figure 2 and shows the type of information recorded for each feature. For example, feature 1 is a new ice-covered fracture that is not covered with snow. The fracture is 12 m wide oriented 90° with respect to the KRMS scan direction. It is frozen with gray ice, it is within a multiyear floe, and its brightness temperature signature is radiometrically warm and of medium contrast with respect to the signature of adjacent multiyear ice.

TABLE 3. Relative Brightness Temperature of Deformational Features With Respect to the Brightness Temperature of Adjacent Ice Measured in Passive Microwave Images

	Number of Features Sampled	Percent of Features Warmer	Percent of Features Cooler	Percent of Features of Same Temperature
All Fractures	115	68.7	13.9	17.4
New fractures	35	40.0	34.3	25.7
Old fractures	80	81.3	5.0	13.7
All Ridges	197	54.8	26.9	18.3
New ridges	61	63.9	6.6	29.5
Old ridges	136	50.7	36.0	13.3
All Features	312	59.9	22.1	18.0
New features	96	55.2	16.7	28.1
Old features	216	62.0	24.5	13.5

The term signature is used throughout this paper to refer to the radiometric characteristics of a particular feature or ice type, usually as imaged with the KRMS microwave radiometer. In most instances, signature is synonymous with 33.6-GHz brightness temperature, and the two can be used interchangeably. In the case of large features or pieces of ice that encompass image areas many pixels in size, signature may also refer to a particular radiometric texture defined by pixel to pixel variation in brightness temperature. In a few instances, signature also refers to the appearance of a feature at optical wavelengths, as in aerial photographs. The context in which the term is used makes clear the particular sensor and medium referred to.

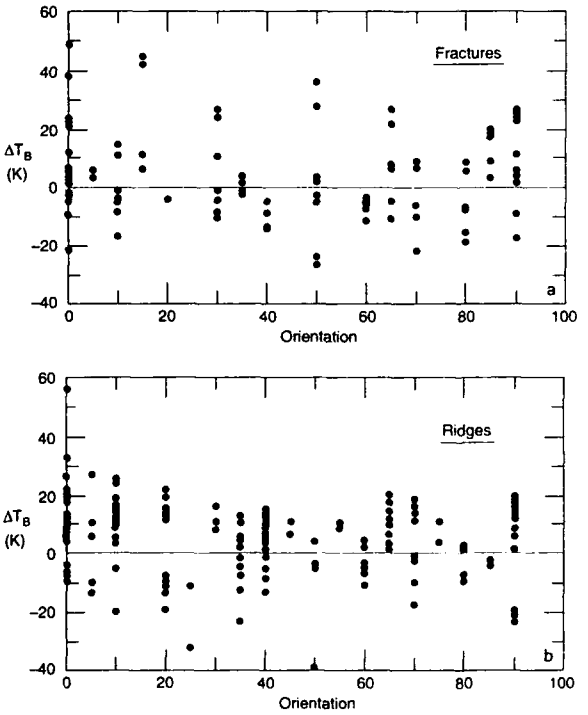

Fig. 3. Effect of feature orientation with respect to KRMS scan direction on radiometric signature. Plots of radiometric contrast as a function of orientation for (*a*) fractures and (*b*) ridges fail to suggest that feature orientation has any effect on signature. Contrast as used in this paper refers to the difference between the brightness temperature of the feature and that of adjacent undeformed ice, signified here by ΔT_B. Features characterized by negative values of ΔT_B are cooler than their background; those with positive values are warmer than their background.

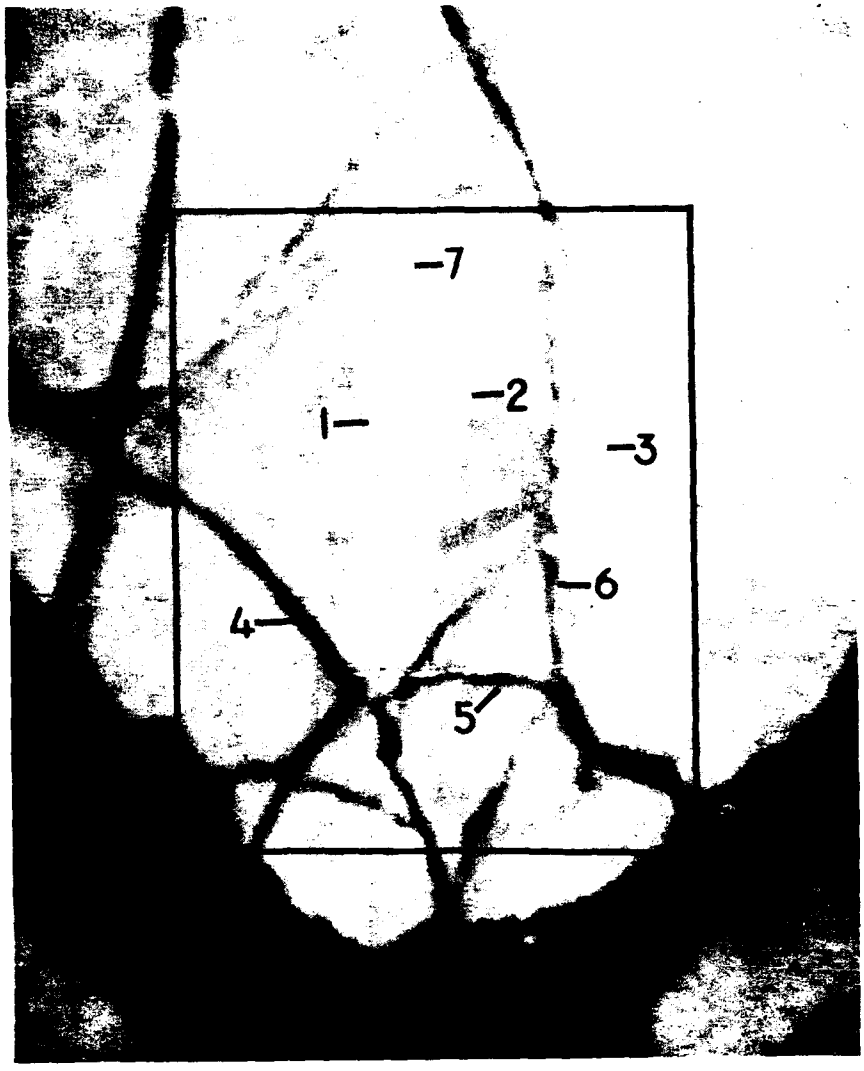

Fig. 4a

Fig. 4. (*a*) Passive microwave image and (*b*) coincident aerial photograph that show ridges with radiometrically cold microwave signatures. Light tones in Figure 4*a* correspond to radiometrically cool features, and dark tones, to radiometrically warm features. The box in Figure 4*a* outlines the approximate area shown in the photograph; use numbers to locate features evident in both media. The distance across the passive microwave scene is approximately 3.6 km.

Many features have clear signatures at both optical and microwave frequencies but some that show clearly in the photograph are not evident in the KRMS data. The opposite is true as well: many linear features evident in the KRMS image lack either sufficient topographic expression to cast shadows or adequate contrast at optical wavelengths and so are not evident in the photograph, which points out one of the benefits of using microwave imagery to detect and map deformational features. For those features that were apparent in KRMS images, the passive microwave signature was described in relative terms as either cooler or warmer than adjacent ice (subsequently referred to here as cool features and warm features), and the apparent contrast of the linear feature with respect to adjacent ice was graded subjectively as low, medium, or high.

During the second phase of analysis, brightness temperature profiles across pressure ridges and fractures were derived from digital passive microwave images. Profiles were measured for a sample of 127 of the 312 features selected in the previous phase of analysis. These profiles, constructed to insure coverage of both the features in question and adjacent sea ice, enable us to determine the level of radiometric temperature contrast between the feature and its background in kelvins. Contrast as used here is simply the difference between the mean brightness temperature of the feature and the mean brightness temperature of background ice. Two contrast values were computed, one each for ice on either side of the feature. Analysis of these data showed that the mean brightness temperature difference between the feature and adjacent ice for the subjective contrast classification used in the first part of the analysis (low, medium, and high contrast, Table 1) is 8.0 K for low-contrast features, 12.1 K for medium-contrast features, and 16.7 K for high-contrast features. The composite matrix of derived contrasts was examined further to assess the effect of feature width, snow cover, ice type, and feature orientation with respect to instrument scan direction on detection of pressure ridges and fractures.

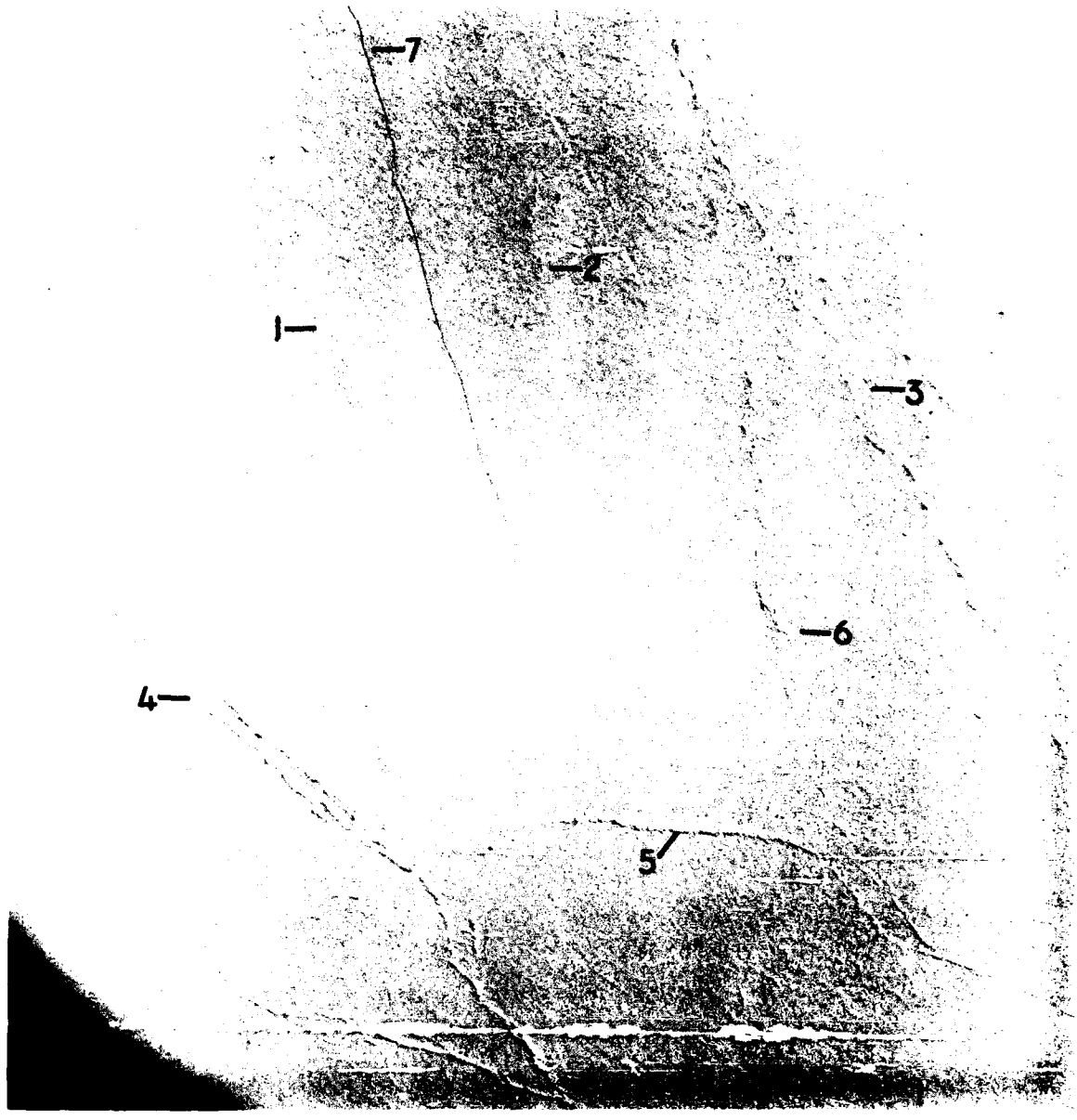

Fig. 4*b*

4. RESULTS

4.1. *Rate of Detection*

Table 2 compares rates of detection of pressure ridges and fractures in passive microwave imagery and summarizes the likelihood of observing deformational features in 33.6-GHz, V-pol passive microwave imagery. Eighty-two percent of all deformational features (fractures and pressure ridges) identified in photographs were resolved in KRMS images. Only 18% of the features had radiometric signatures of such low contrast that they could not be observed at all in the passive microwave data (e.g., contrast poorer than feature 2 in Figure 2*a*). Fractures and ridges have equal likelihoods of detection. In general, old deformational features are more likely to be detected than new features, but not by a substantial margin.

4.2. *Brightness Temperature Characteristics*

Table 3 summarizes relationships observed between the brightness temperature of deformational features and that of adjacent ice. Radiometric signatures of both fractures and pressure ridges are more likely to be warmer, rather than cooler, than adjacent ice. In general, fractures are more likely to be radiometrically warm (220 to 250 K in KRMS data) in comparison with adjacent ice than are pressure ridges (Table 3). This reflects the fact that frozen fractures almost invariably are saline ice regardless of the character of adjacent ice, whereas ridges that form in multiyear ice probably are composed at least in part of blocks of radiometrically cool (170 to 210 K in KRMS data) multiyear ice (that contains little brine) as well as blocks of saline first-year ice. New ridges are more likely to be warm than are old ridges, which suggests that ridges cool radiometrically as

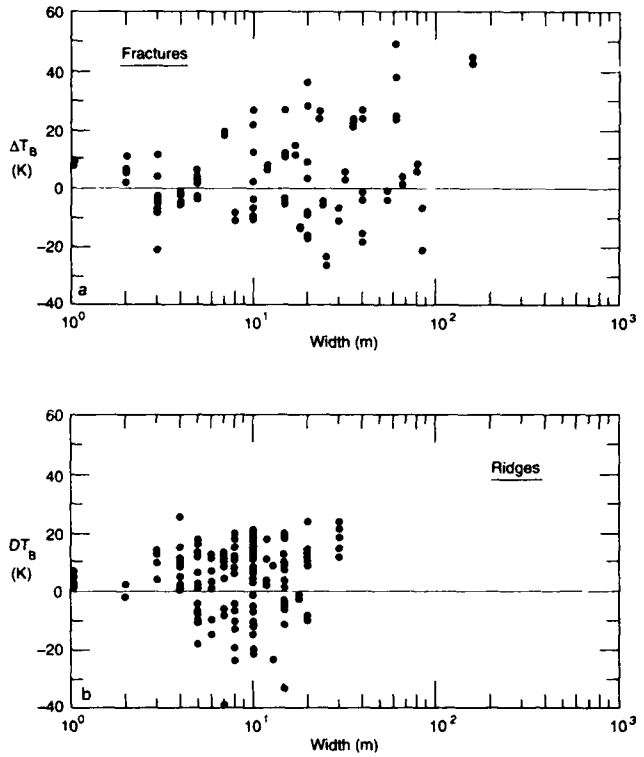

Fig. 5. Radiometric contrast ΔT_B plotted as a function of log feature width for (*a*) fractures and (*b*) ridges. The range of contrast increases with feature width, although many wide features show low contrast and some features far narrower than the sensor beam spot (26 m) show remarkably large contrast. Both classes of features, ridges and fractures, show similar contrast characteristics.

they age. Old fractures tend to be warmer than new fractures for reasons that are not fully understood. In fact, only 5% of old fractures observed in the data were radiometrically cooler than adjacent ice.

4.3. *Radiometric Contrast*

Table 4 summarizes relationships in radiometric contrast observed between deformational features and adjacent ice. Most features examined are characterized by high radiometric contrast with respect to adjacent ice (e.g., features 3 and 6 in Figure 2*a*). Old features typically show higher contrast than new features and include fewer features that show no radiometric contrast with adjacent ice. The probability of detecting a feature thus increases with feature age. New fractures are least likely to be detected because they include the lowest percentage of high-contrast features (20%) and the highest percentage of low-contrast features (54%) of all feature classes studied. In addition, a significant fraction of features in the new fracture sample (25%) show no contrast with adjacent ice. Thus 80% of new fractures studied are characterized by low contrast or by no contrast signatures, as compared with 55% of new ridges, 37% of old ridges, and only 27% of old fractures. This result might arise from the poor resolving power of the microwave sensor relative to that of the camera. Many narrow fractures which show clearly in photographs do not cover a sufficient fraction of the sensor beam spot to have significant effect on the microwave signal, even if ice within the fracture shows good radiometric contrast with adjacent ice.

4.4. *Feature Orientation With Respect to Scan Direction*

The effect of the orientation of a feature with respect to the direction of sensor scan on its likelihood of detection was investigated. Experience with infrared sensors that, like KRMS, typically build images using a scanning mechanism suggests that the orientation of a feature may be critical to its detection. There is evidence as well that ridge detection with active microwave sensors is dependent on feature orientation [*Leppäranta and Thompson*, 1989].

Scan direction in KRMS images is across the scene, parallel to pixel rows in the image, and perpendicular to the direction of flight. The angle at which features are inclined with respect to scan direction was measured manually on hard copy images using the orientation of pixel rows for reference. Values of orientation range from 0°, for features oriented parallel to scan direction, to 90°, for features oriented perpendicular to scan direction. Radiometric contrast, when plotted as functions of feature orientation for ridges and fractures, fails to show systematic trends (Figure 3). (Radiometric contrast (ΔT_B) used here and in subsequent figures is the difference between mean brightness temperatures measured for the ridge or fracture and those of adjacent flat-lying ice. Each feature thus is associated with two contrast values, one each for ice on either side of the feature.) If feature signatures were dependent on their orientation within the scene, contrast would be expected to increase (or decrease) with angle. Or, if detection was enhanced at preferred angles, contrast should form peaks at some angles and valleys at all others. Neither effect is observed. This result thus suggests that detection of linear features in KRMS images is independent of their orientation.

4.5. *Feature Width*

Feature width affects radiometric contrast in cases where the fracture or ridge does not fill the instantaneous sensor footprint completely. In such case the radiance measured is a function of (1) the brightness temperatures of the feature and adjacent ice and (2) the percentage of the footprint covered by each. The instantaneous 3-dB KRMS beam spot for data used here is approximately 26 m in diameter. A feature thus must be at least 52 m wide to insure that it fills at least one 3-dB beam spot completely, although a feature as narrow as 26 m also will fill the beam if it is centered precisely with respect to the footprint digitized within a given pixel.

All of the ridges and most of the fractures investigated here are narrower than 26 m. Though these features are not resolved in full radiometric and spatial detail, they are characterized nonetheless with surprisingly good radiometric contrast (e.g., Figures 2*a* and 4*a*). Figure 5 shows radiometric contrast plotted as a function of log feature width for both fractures and ridges. Fractures and ridges behave similarly; neither shows a trend toward high-contrast features over the other. Features greater than 10 m wide show essentially the same range of contrast as the broadest features sampled (approximately ±40 K). Contrast decreases with width for features narrower than 10 m, as is to be expected when dealing with subresolution scale sizes, but features 1 m wide still show brightness temperatures that deviate from those of adjacent ice by as much as 10 K.

Figure 6 shows two examples of these narrow features,

each of which appears in the scene in Figure 2 (features 2 and 5). Both are frozen cracks less than 1 m wide in a multiyear floe. Their passive microwave signatures are distinct even though their apparent widths are far smaller than KRMS' 28-m beam spot. Both cracks are radiometrically warmer than adjacent multiyear ice and have apparent contrasts of approximately 12 K. A similar signature is observed for the narrow crack imaged in the scene in Figure 4 (feature 7). The fact that these extremely narrow features are portrayed with distinct signatures in the passive microwave data serves to emphasize the point that this class of sensors is poorly suited to applications requiring accurate measurement of feature width, a point first suggested by *Ketchum et al.* [1983]. Although few of the features analyzed here are this narrow, few are wider than the sensor beam spot yet most have clearly defined signatures (Table 4, Figure 5).

4.6. *Feature Age and the Presence of Snow*

Here we attempt to determine, within limits that the data permit, the extent to which snow alters fracture and ridge signatures. Of the fractures investigated in the second phase of the study, 51% were snow-covered and 73% of the ridges had substantial snow drifts associated with them. Radiometric signatures of these snow-covered features are compared with signatures of snow-free features in Figure 7, where radiometric contrast is plotted as a function of brightness temperature for fractures and ridges.

Snow cover has little apparent effect on fracture signatures as evidenced by the similar spread in contrast and brightness temperature for snow-covered and snow-free points (Figure 7*a*). Snow-free fractures show a slightly broader range of brightness temperatures than snow-covered fractures, but the number of observations outside the range of brightness temperatures observed for snow-covered fractures is small. Brightness temperatures of snow-covered ridges, on the other hand, vary over a significantly broader range than those measured for snow-free ridges (Figure 7*b*). Snow-covered ridges are as much as 15 K warmer and 20 K cooler than the warmest and coolest snow-free ridges. Radiometric contrast measured for ridges, nonetheless, does not appear to depend on snow cover.

It is important to note that the sample of snow-covered fractures is biased toward fractures frozen with thick ice (ice greater than 25 cm thick, the approximate thickness at which sea ice sustains a snow cover [*World Meteorological Organization* (*WMO*), 1970]). Snow falling on thin ice either melts rapidly as a result of wicking or the presence of surface brine, or depresses the ice surface below freeboard and causes flooding. Other work suggests that melting, wicking, and flooding produce marked changes in radiometric signature [*Tucker et al.*, 1991; *Lohanick*, 1993]. Imagery analyzed here was obtained under cloud-free conditions and does not include examples of thin ice undergoing active precipitation. As a consequence, snow-covered thin ice is not represented in the data set.

4.7. *Discrimination Between Fractures and Pressure Ridges*

Fractures and ridges show similar ranges of contrast and brightness temperature; neither shows any tendency to fall within a discrete, well-bounded cluster (Figure 8). Discrimination between fractures and ridges using brightness temperature and radiometric contrast thus does not show promise. Figure 9 shows a representative sample of mean brightness temperature profiles measured across ridges and fractures. Visual comparison between the shapes of these and other profiles derived from the data set shows that fracture and ridge profiles are similar; profiles from neither class show distinctive features that would provide a basis for discrimination. This result may well reflect the fact that the width of most features analyzed here is narrower than the beam spot of the passive microwave sensor (Figure 5). Radiometric differences between ridge and fracture profiles may well exist at fine spatial scales, but current state-of-the-art aircraft sensors lack sufficient resolving power to be effective at resolving them.

Although automated discrimination between ridges and fractures using radiometric information alone does not seem promising, visual examination of passive microwave images suggests that linear features associated with deformation can be classified with reasonable accuracy using conventional image interpretation methods. For example, the position of a feature with respect to floe boundaries, its length, continuity, and uniformity of width, its relationship with respect to features that cross it, and its location within the Arctic Basin all provide relevant information lacking from radiometric descriptors analyzed here. Even in the absence of reliable methods to discriminate fractures from ridges, the ability to recognize deformational features as a class is an important contribution.

5. DISCUSSION

Radiometric contrast ultimately is the primary variable that determines whether a feature can be detected or observed. It is important therefore to understand processes and variables that affect the brightness temperature of the feature and adjacent ice and that determine brightness temperature relationships summarized in Tables 2 through 4, shown in Figures 3, 5, 7, 8, and 9, and discussed in section 4. Processes associated with the formation of fractures and pressure ridges establish the character of initial radiometric signatures associated with these deformational features. The type of ice adjacent to the feature and local characteristics of the snowpack determine the initial radiometric contrast between the feature and its background. Subsequent accumulation of snow and processes of aging related to snow metamorphosis and ice growth and decay alter these signatures. We offer the following conceptual models, based on results discussed above, for understanding microwave signatures of ridges and fractures.

5.1. *Ridge Signatures*

Ridge signatures are complex. Ridges occur in sea ice of all thicknesses, ages, and salinities. They may be composed entirely of ice similar in composition and thickness to ice adjacent to the ridge, or of ice of completely different character. Whether a ridge can be detected in a passive microwave image depends on the radiometric contrast between ice within the ridge and ice adjacent to it. Radiometric contrast, in turn, is a function of the electromagnetic properties of ridge ice taken with respect to those of adjacent ice.

Figure 10 depicts three general types of ridges in schematic form, developed from an unpublished report on pres-

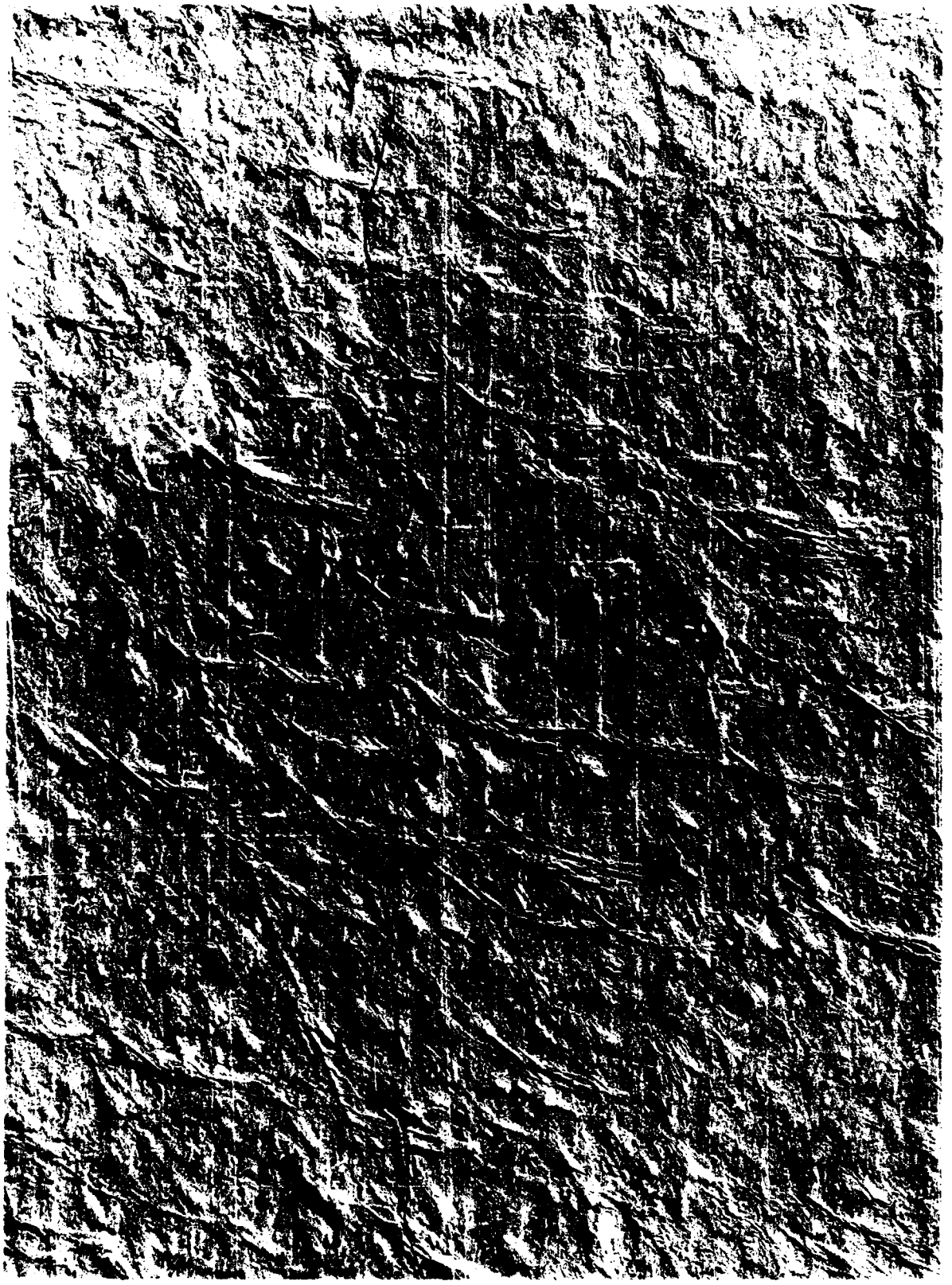

Fig. 6*a*

Fig. 6. Enlargements of selected areas of the photograph in Figure 2*b* showing cracks designated as features (*a*) 2 and (*b*) 5 in Figure 2 and Table 1. Boxes drawn on Figure 2*b* indicate the area shown in each enlargement. Each enlarged scene shows an area approximately 350 by 475 m in size.

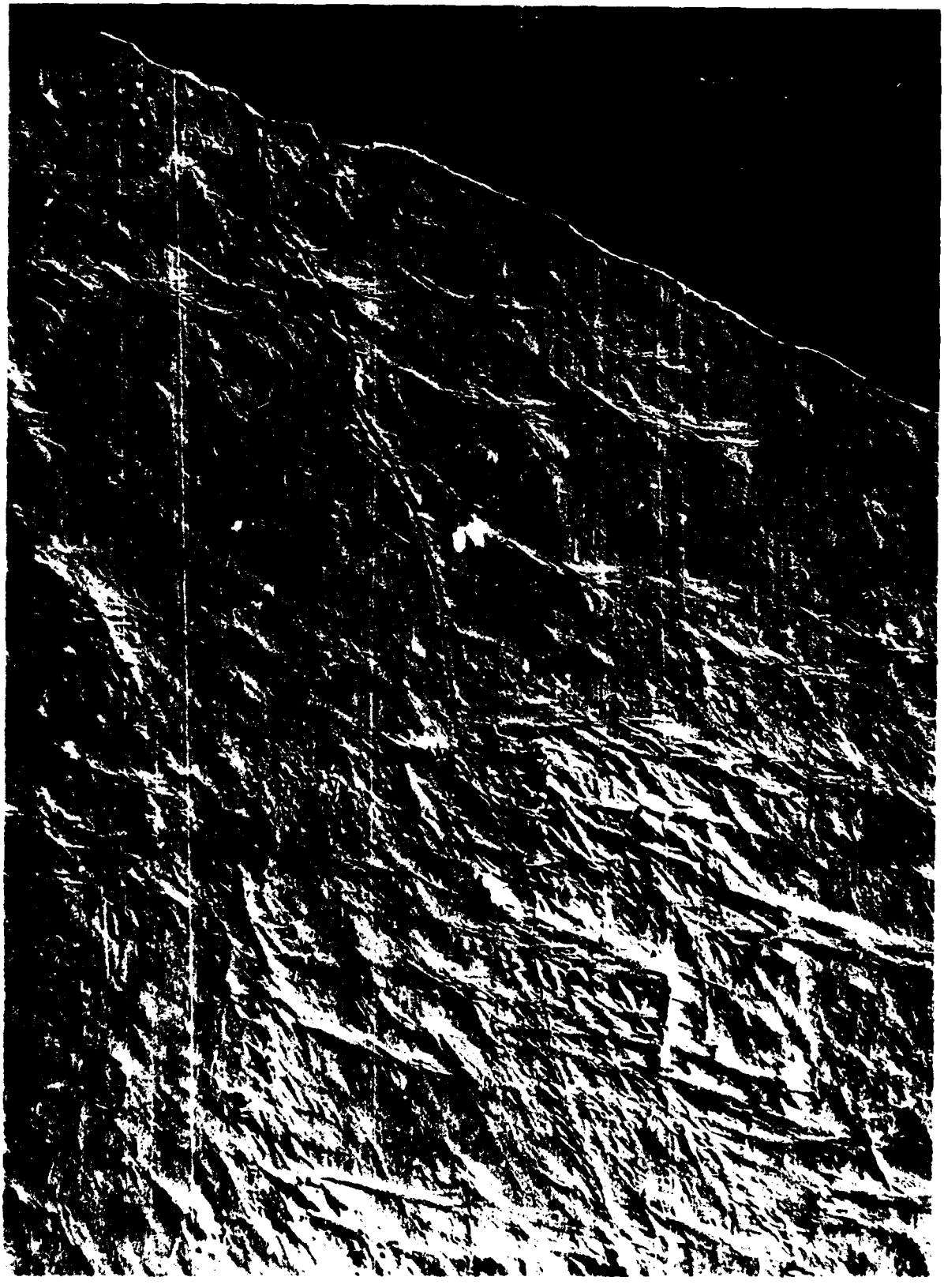

Fig. 6b

sure ridges by W. F. Weeks and A. Kovacs. Aerial photographs and coincident passive microwave images in Figure 11 show examples that we interpret to be representative of each of the three ridge types. The different types of ridges are distinguished both by physical characteristics of ridge ice and adjacent ice and by the location of the ridge (whether it occurs in the middle of a generally uniform sheet of ice or at the boundary between two different types of ice).

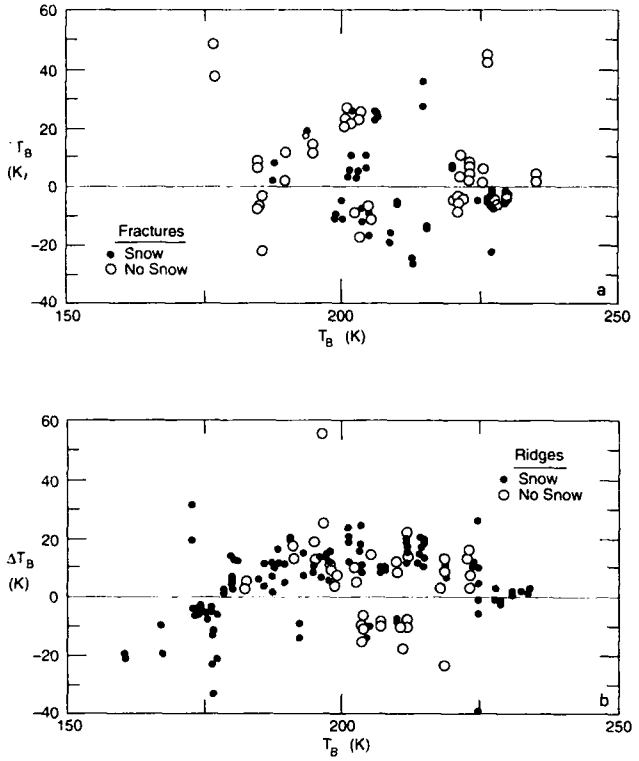

Fig. 7. Radiometric contrast (ΔT_B) plotted as a function of brightness temperature (T_B) for snow-free features and snow-covered features: (*a*) fractures, and (*b*) ridges. These data suggest that snow has no apparent effect on fracture signatures. However, signatures for snow-covered ridges extend over a broader range of brightness temperatures than signatures for snow-free ridges, although the range of radiometric contrast is similar for both snow-covered and snow-free ridges.

In the first case a radiometrically warm sheet of first-year ice that covers a frozen lead is compressed between thicker and radiometrically cooler sheets of multiyear ice (Figure 10*a*). The ridge that results is composed almost exclusively of blocks of radiometrically warm first-year ice derived from the frozen lead. First-year ice in the ridge presents a contrasting target when set against the adjacent, radiometrically cool, low-salinity multiyear ice. Ridges of this type thus show distinct signatures in passive microwave images, particularly when they are newly formed (Figure 11*a*). Note, however, that it may be difficult to distinguish this type of ridge from a narrow ice-covered lead that is not deformed.

In the second case an ice sheet fails and a ridge forms without creation of an intermediate ice sheet in the zone of fracture (Figure 10*b*). The failed ice sheet may be either multiyear ice, first-year ice, or some form of thin, newly formed ice. Because ridge ice in this case consists of ice of the same thickness and physical character as adjacent ice, initial radiometric contrast between the ridge and adjacent ice is low or nonexistent. Detection of these features in passive microwave images is unlikely, especially if the ridge formed recently (Figure 11*b*).

In the third case a ridge forms at the boundary between ice sheets of different composition and thickness (Figure 10*c*). This situation typically occurs at the edge of multiyear floes that are surrounded by first-year ice. The ridge that results may be composed of blocks of either ice type, and in most instances both first-year ice blocks and multiyear ice blocks probably are present. In the case where the ridge is composed of a mixture of ice types the ridge will have a brightness temperature that is intermediate between that of multiyear ice and first-year ice and so have some degree of radiometric contrast. But because the ridge is located at the juncture between the two ice sheets, its presence will be difficult to detect (Figure 11*c*). The slope of the radiometric gradient across the boundary might be reduced slightly (Figure 10*c*), but the ridge signature is unlikely to be distinguished unambiguously from the signature that typified the boundary before the ridge formed.

Each of these examples assumes that ice adjacent to the ridge is undeformed and that its signature is not altered by ridge-forming processes. In fact, surface observations suggest that ice along the trend of pressure ridges commonly is fractured and, in some cases, warped downward into a monocline to form a trough [*Fukutomi and Kusunoki*, 1951; *Breslau et al.*, 1970; *Hanson*, 1980]. The trough may become flooded, or overlying snow may wick up moisture [*Lohanick*, 1993] (Figure 12). The trough thus may well have a signature of its own that, although spatially separate from the ridge proper, defines a linear feature that contrasts radiometrically with the ridge on one side and adjacent ice on the other. Development of these troughs may be a critical factor in detection of some ridges, especially those described by the second case above (Figure 10*b*).

Most ridges observed in the Arctic can be interpreted within the context of these examples. Signatures within each class can be expected to show a certain degree of variability. For example, ridges described by the first and third cases (Figure 10*a* and 10*c*) most likely consist of mixtures of multiyear ice and first-year ice. Results presented above show that ridge signatures typically are warmer radiometrically than signatures of background ice (Table 3), suggesting that saline ice, which is radiometrically warm, is a constituent of most ridges, either as blocks of first-year ice or as blocks of multiyear ice that have been uplifted, tilted, or overturned so that their high-salinity undersides face skyward toward the passive microwave sensor. The relative proportion of saline ice to fresh ice, which determines the emissivity integrated over the sensor footprint (bulk emis-

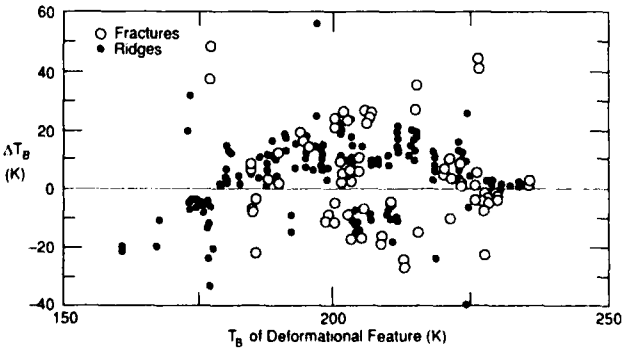

Fig. 8. Radiometric contrast (ΔT_B) plotted as a function of brightness temperature (T_B) for ridges and fractures. Ridges and fractures display similar ranges of contrast and temperature, and neither class of features shows a tendency to plot within a discrete, well-bounded cluster. This suggests that these features cannot be distinguished from each other if simple measures of brightness temperature or radiometric contrast are the sole criteria used for discrimination.

sivity) and thereby the brightness temperature signature, is likely to vary from ridge to ridge, or even from point to point on a single ridge.

Perhaps more significant in terms of signature variability are time-dependent effects of aging. Brightness temperature signatures observed for new ridges are warmer than those of old ridges (Table 3), which suggests that aging processes reduce the radiometric temperature of ridges. Such changes in brightness temperature alter radiometric contrast between

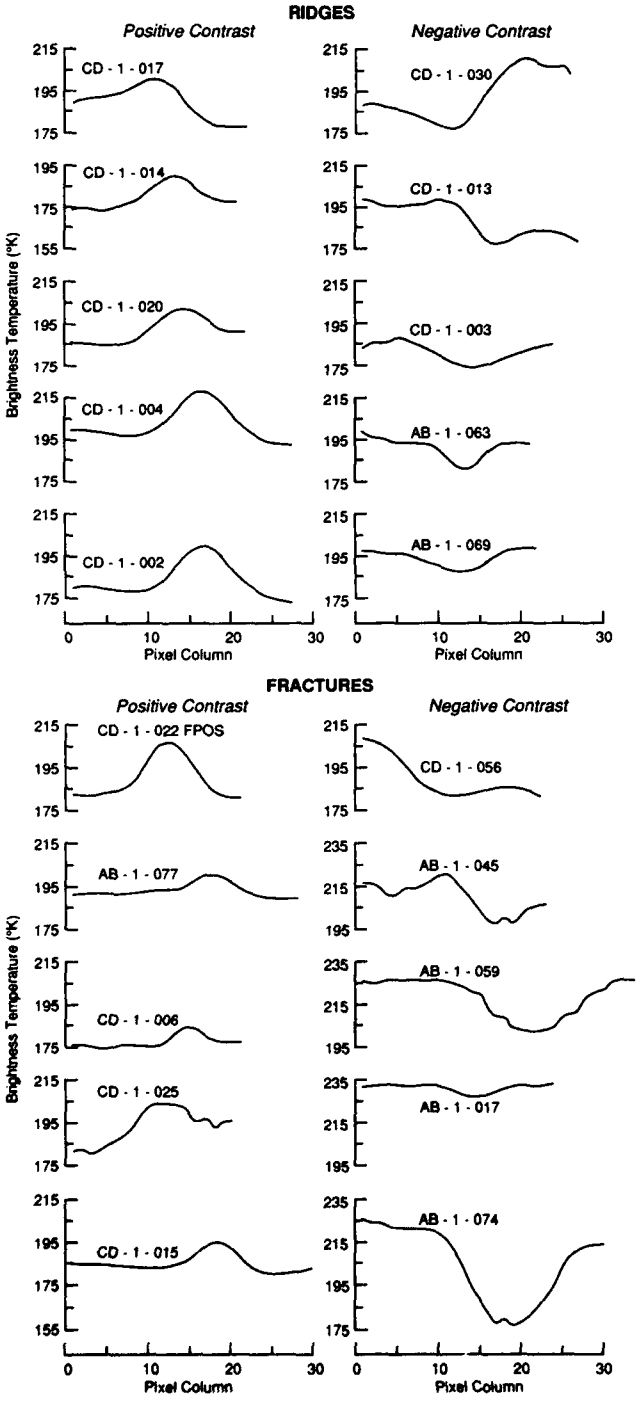

Fig. 9. Representative profiles of mean brightness temperature measured across fractures and pressure ridges. Neither ridges nor fractures show distinctive characteristics that can be used to distinguish one type of feature from the other.

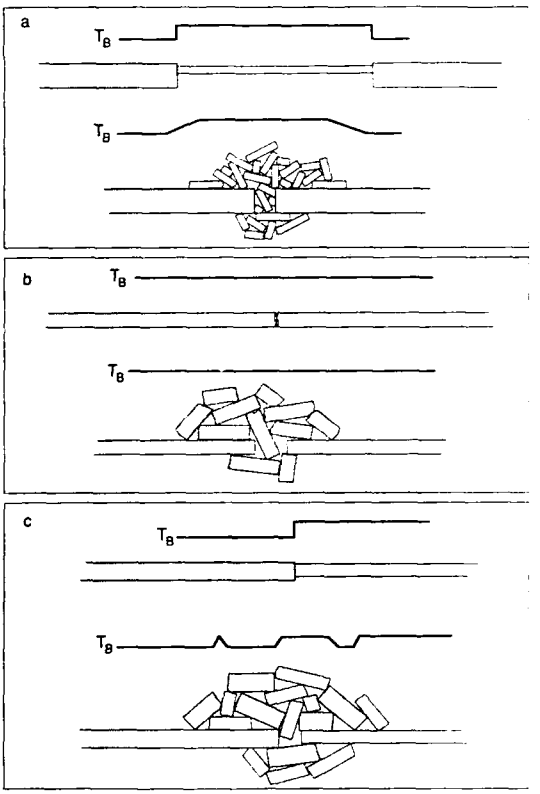

Fig. 10. Generalized drawing of three classes of ridges (after W. F. Weeks and A. Kovacs, unpublished report circa 1970) and their predicted passive microwave profiles before and after formation of the ridge (dark line above each drawing). (*a*) A ridge composed of first-year ice (white) forms between multiyear floes (gray). The ridge signature contrasts with that of adjacent ice. (*b*) A ridge forms within a floe. The ridge signature is the same as that of adjacent ice. (*c*) A ridge forms at the boundary between two ice types characterized by contrasting radiometric properties (e.g., multiyear ice in gray, and first-year ice in white). The ridge signature includes elements of both adjacent ice types.

the ridge and adjacent ice, which in turn affects the likelihood that the ridge will be observed. Temporal changes in radiometric contrast associated with ridge signatures probably evolve along two general tracks, depending on whether the ridge is composed of first-year ice or young ice and occurs within a multiyear floe (Figure 10*a*) or whether the ridge is composed predominantly of ice similar to the adjacent ice sheet (Figure 10*b*) (i.e., a ridge of first-year ice within a sheet of first-year ice, or a ridge of multiyear ice within a multiyear floe).

In the case of ridges composed of first-year ice within a radiometrically cool multiyear ice floe (Figure 10*a*), radiometric contrast is at a maximum soon after the ridge forms and decreases with time as the brightness temperature of the radiometrically warm, saline ridge cools. We speculate that as brine drains from upturned blocks, the bulk emissivity of the ridge declines, a process that would produce greatest change in signatures of ridges composed predominantly of first-year ice. We also speculate that accumulation of snow against the ridge, growth of depth hoar within the snow pack, and formation of hoar frost within cavities between blocks of ice in the ridge probably enhance scattering. Reduced emissivity and increased scattering both reduce radiometric temperature.

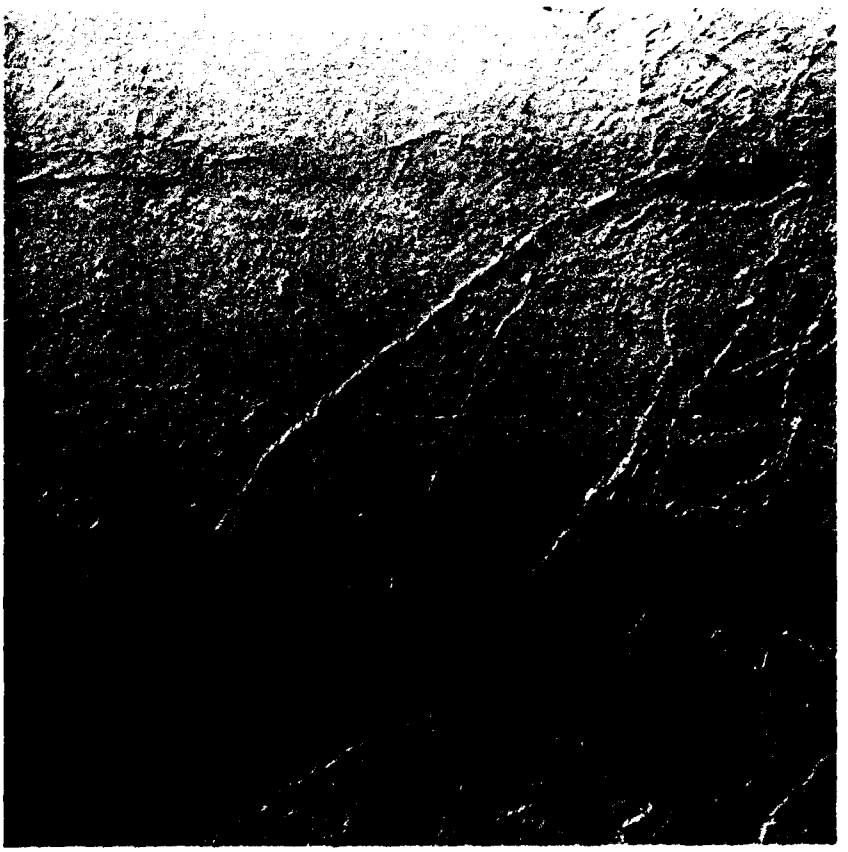

Fig. 11*a*

Fig. 11. Aerial photographs and coincident passive microwave images (KRMS) that show examples of the three classes of pressure ridges drawn schematically in Figure 10. (*a*) Ridge composed of first-year ice in a multiyear floe has a high-contrast signature. (*b*) Ridges composed of gray-white ice surrounded by undeformed gray-white ice have little or no radiometric contrast. (*c*) Ridges at the edge of floes have no radiometric contrast. Each scene is approximately 1280 m on a side.

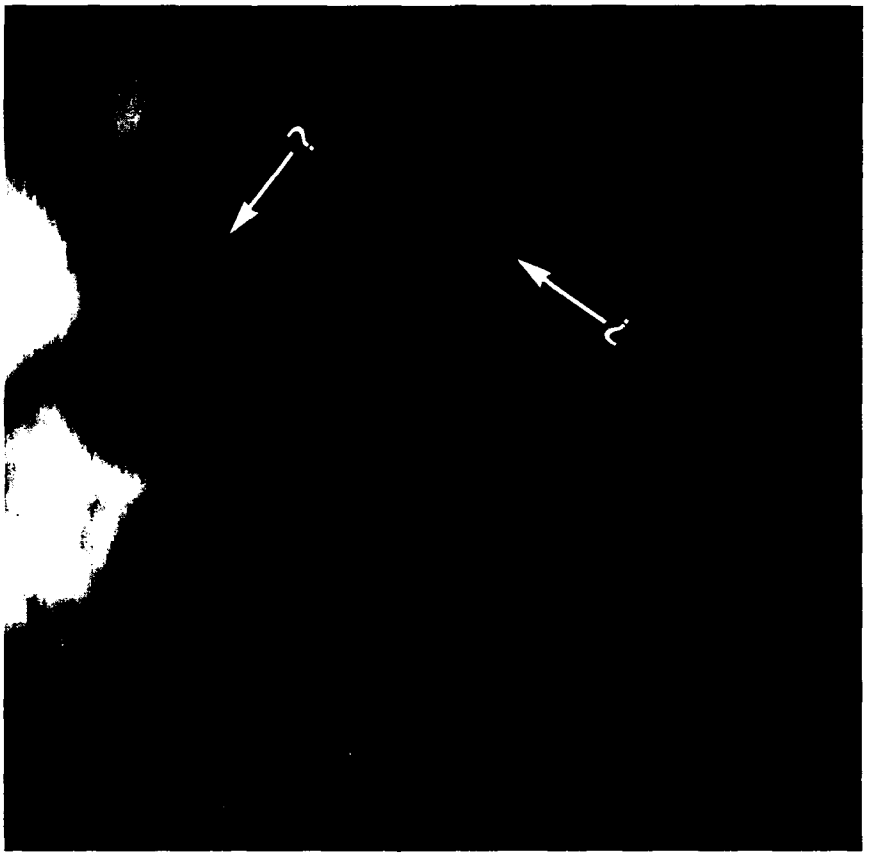

Fig. 11b

Fig. 11c

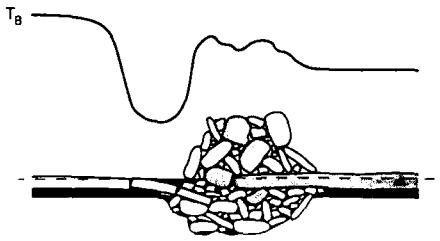

Fig. 12. Generalized drawing of ridge with adjacent trough flooded with seawater [after *Fukutomi and Kusunoki*, 1951]. The ridge consists of blocks of first-year ice (white) and multiyear ice (gray) derived from the colliding ice sheets. Flexure of thinner ice is sufficient to depress it below freeboard near the ridge. Seawater fills the trough that results. The black line above the drawing traces the predicted brightness temperature profile across the ridge.

At some point the brightness temperature of the ridge presumably declines to that of adjacent ice, and the feature can no longer be detected. Whether this degree of cooling can be achieved in one winter is not clear because rates at which these processes proceed are undocumented. It also is not clear whether this class of ridges can continue to cool beyond the brightness temperature of adjacent ice after desalinization is complete. Presumably, brightness temperature could continue to decline in response to progressive development of scatterers in the snow pack and voids between ridge blocks, in which case the ridge would eventually reemerge as a radiometrically cool feature with respect to adjacent ice.

Radiometric contrast of ridges composed of ice derived from the adjacent undeformed ice sheet (Figure 10*b*) follows a different pattern of change with time. When the ridge is created, contrast is minimal because the ridge and adjacent ice are composed of essentially the same material. As the ridge ages, however, its brightness temperature signature is likely to change differentially with respect to that of adjacent flat-lying, undeformed ice owing to inherent structural differences. Topographic relief, blocky structure, and cracks in ice that parallel the ridge trend tend to enhance brine drainage, snow entrapment, porosity and permeability of the ice sheet, and vapor transport. We speculate that these factors foster temporal changes in emissivity and development of scatterers to an extent not possible over the same period of time in adjacent undeformed ice. The brightness temperature of adjacent ice will continue to evolve, but through processes that are different from those that affect the radiometric signature of the ridge.

Radiometric differences observed between snow-free and snow-covered ridges (Figure 7*b*), which suggest cooling with age, are consistent both with this model and with previous work. Brightness temperature profiles measured across first-year ice by *Lohanick and Grenfell* [1986] show a general correlation between snow depth and brightness temperature at K_a-band frequencies (V-pol) for snow depths greater than 80 cm. Data obtained by *Lohanick and Grenfell* [1986] in another experiment show that removing snow from a sheet of undeformed first-year ice raised the brightness temperature by approximately 15 K. Analyses of effects of terrestrial snow packs suggest radiometric cooling of up to approximately 20 K as a result of scattering from well-developed depth hoar layers within the snow pack [*Hall et al.*, 1982, 1986]. Scattering models and radiative transfer models predict similar results [*Kong et al.*, 1979; *Ulaby and Stiles*, 1980; *Fung and Chen*, 1981; *Hall*, 1987].

Whereas snow probably mediates the brightness temperature and radiometric contrast of most ridges, it probably plays an insignificant role in determining signatures of ridges with the coolest brightness temperatures. The coolest ridges observed in the data set correspond to features that lack significant topographic relief and so are difficult to observe in photographs. We interpret these features as the roots of old, annealed, relict ridges that have lost surface expression through multiple episodes of melt and that are composed of ice that is significantly different from adjacent ice that grew in place and has not been substantially deformed. Signatures of these features commonly are between 10 and 20 K cooler than adjacent multiyear ice in which they occur (Figure 4; *Eppler et al.* [1986]), but in some instances the contrast approaches 30 K.

Physical processes that produce radiometric cooling of this magnitude (10–20 K) in ice without marked topographic relief are neither well documented nor well understood. We speculate that the extremely cool brightness temperature signature is related to enhanced scattering from annealed ridge ice. Surface measurements presented by *Grenfell* [1992] show that the winter emissivity of multiyear ice is related to the thickness of the low-density scattering layer that develops at the ice surface during summer melt. Grenfell shows that emissivity decreases with increasing thickness of this layer. The crystalline structure of annealed, metamorphosed ridge ice may be such that it fosters development of either a thicker low-density layer than is present on adjacent ice, or a layer with unique structure that produces enhanced scattering of microwave energy at K_a band frequencies.

5.2. *Fracture Signatures*

Initial failure of sea ice is almost always due to tension [*Assur*, 1963]. Shear and compression follow in many instances, or tension persists and the crack widens to form a lead. Lead and fracture signatures are characterized by great variability during the relatively brief period when exposed water is freezing and the ice cover is developing [*Eppler et al.*, 1986; *Grenfell et al.*, 1988]. Once a continuous ice sheet forms across a fracture, brightness temperatures remain relatively stable and show only gradual change with time.

Open water exposed in the lead or fracture is a poor emitter ($E \approx 0.5$) and thus appears radiometrically cold to passive microwave sensors (140–150 K (J. P. Hollinger, personal communication, 1990)), colder in fact than any of the different types of sea ice commonly encountered [*Troy et al.*, 1981; *Eppler et al.*, 1986]. Initially, while unfrozen, fractures and leads thus appear cold radiometrically. Saline ice, in contrast to open water, is highly emissive ($E \approx 0.95$) and radiometrically is the warmest surface observed in most Arctic images. As dispersed ice crystals (frazil) form in the water column and float to the surface, the radiometric temperature sensed over the lead rises. In general the brightness temperature at any given time is roughly proportional to the percent of the surface within the sensor footprint that is covered by ice, although the precise relationship between partial ice coverage and brightness temperature remains unresolved. When the entire surface is covered to a depth equal to approximately twice the sensor wavelength, the surface reaches a maximum brightness temperature

equal to that of saline ice [*Eppler et al.*, 1986; *Grenfell et al.*, 1988].

The brightness temperature of the continuous ice cover remains radiometrically warm for the duration of the winter, although some cooling may occur. Initially, this radiometric cooling occurs both in response to consolidation and roughening of the ice surface and as a result of thermal cooling of the surface as freeboard increases and as the skin depth seen by the sensor cools from sea surface temperature (typically −1.8°C) to ambient air temperature. Subsequent long-term radiometric cooling may occur over the course of the winter owing to metamorphosis of the snow cover [*Hall et al.*, 1982, 1986; *Hall*, 1987], development of surface scatterers at the snow-ice interface [*Eppler et al.*, 1990; *Lohanick*, 1993], or general effects of aging and growth of the ice sheet.

Lack of apparent differences between radiometric signatures of snow-covered and snow-free fractures analyzed here (Figure 7*a*) runs counter to the apparent effect of snow on ridge signatures described above (Figure 7*b*) and contradicts previous work which relates snow cover to changes in radiometric signature [e.g., *Hall et al.*, 1982, 1986, *Hall* 1987; *Lohanick and Grenfell*, 1986; *Lohanick*, 1993]. The difference might be due to the nature of snow covers associated with fractures and ridges. Aerial photographs show that snow associated with ridges included in this study commonly occurs as drifts, some of which appear to be quite deep, which according to *Lohanick and Grenfell*'s [1986] data would favor radiometric cooling. Snow on fractures typically occurs as a relatively uniform sheet, albeit with local variations in thickness, that is far thinner than the drifts associated with ridges. Although drifts occur at lead edges where wind deposits snow against thicker ice, brightness temperatures used in this analysis to characterize fractures are representative of the broad section of flat ice overlain by a thin snow cover, not ice at lead edges where drifts occur.

Additionally, ridges also are the site of incompletely healed ruptures in the ice cover which form conduits for exchange of heat and vapor, both agents of metamorphosis in snowpacks which favors enhanced scattering and cooler signatures. Though leads too are sites of rents in the ice cover, lead ice is far more continuous than blocks in a ridge and forms an effective seal that inhibits exchange of heat and vapor. Scattering from snow thus may play a less dominant role in the temporal evolution of fracture signatures.

Fracture and lead signatures can be classified into three categories that are defined on the basis of the stage of development of the ice cover in the lead. First, newly formed fractures that expose open water are characterized by brightness temperatures that are lower than other naturally occurring surfaces observed in the Arctic (Figure 13*a*). Second, fractures that are in the process of freezing and that are incompletely covered with ice are characterized by brightness temperatures that increase with time and span a broad range from very cool to very warm (Figure 13*b*). Third, fractures that are frozen completely are radiometrically warm (Figures 13*a* and 13*b*).

The first two classes of fracture and lead signatures, which arise from open water and an ice cover which is incompletely frozen and commonly are ephemeral, short-lived stages, particularly when the air temperature and wind speed are low and differential motion of the ice pack is slight. Signatures that typify both classes of features are well defined and easily recognized, owing both to the unique brightness temperature of open water and to textural aspects of accumulating ice covers [*Eppler and Farmer*, 1991]. Neither class of features occurs in great abundance at any given time in the winter pack. Nor are they well represented in the sample of features analyzed above.

The third class is characterized by warm radiometric signatures that persist until melt ensues and brine is flushed from the ice surface. Detection of these fractures depends primarily on radiometric characteristics of ice adjacent to the fracture. For example, mature fractures are difficult to detect if they occur within first-year ice, but they leave clearly defined signatures if they occur in multiyear ice because of the radiometric contrast between radiometrically warm lead ice and cool old ice. Microwave signatures of the meter-wide cracks in multiyear ice noted above (Figures 2 and 4) demonstrate this point.

We hypothesize that subresolution-scale cracks such as these are detected by the passive microwave sensor for three reasons. First, the warm brightness temperature of saline ice within the cracks differs significantly from the cool brightness temperature of adjacent multiyear ice. Even though the area subtended by the crack comprises a relatively small fraction of the footprint area, the radiance of emissive first-year ice which fills the crack makes a significant contribution to the integrated radiance measured over the full footprint.

Second, cracks in Figures 2 and 4 are associated with linear, continuous signatures. Brightness temperatures of the crack signatures are relatively uniform along the length of each feature, which makes them easy to detect. If ice covering the cracks were discontinuous or if the shape of the features were such that they involved small, isolated groups of pixels, then it would be more difficult to recognize them as discrete, continuous features among the mottled radiometric texture typical of multiyear ice.

Third, deformational processes that created the crack might also have altered the physical structure and dielectric properties of adjacent ice and snow. These changes could be manifest as radiometrically warm signatures for ice immediately adjacent to the ridge [*Ketchum and Lohanick*, 1980]. For example, Figure 6*b*, which is an enlargement of the portion of the photograph in Figure 2 that includes the crack labeled as feature 5, shows that small ridgelike features, with sufficient relief to trap blowing snow, have developed along the edge of the crack. Figure 6*a* shows similar, less well developed ridges along some segments of the feature labeled 2 in Figure 2. The observed microwave signatures thus may emanate from an area that is somewhat broader than the crack trace that is visible in photographs.

6. Summary and Conclusions

On the basis of analysis of K_a band (33.6 GHz, V-pol) passive microwave images and coincident aerial photographs we make the following conclusions.

1. Most deformational features are resolved in airborne passive microwave imagery.

2. Radiometric signatures of both fractures and ridges are more likely to be radiometrically warmer than adjacent ice (as opposed to cooler), which suggests that saline ice is a constituent of most deformational features.

3. New ridges are more likely to be radiometrically warm than old ridges.

Fig. 13*a*

Fig. 13*b*

Fig. 13. KRMS passive microwave images of a freezing lead in the Beaufort Sea. Two images, which show the same fracture, were acquired 6 hours apart on March 11, 1988, at approximately 73°N, 142°W. Both images were obtained from an altitude of 6100 m and show areas approximately 14.5 km × 9.6 km in size. Tracks flown were not exactly coincident, so images overlap only down the central part of the figure. Dark tones mark surfaces that are highly emissive and radiometrically warm (new ice and first-year ice). Light gray tones correspond to surfaces characterized by low emissivity and cool brightness temperatures (multiyear ice, open water). (*a*) The fracture, which is the sinuous, light gray stripe that extends across the center of the image, exposes open water. The gray band along the lower edge of the fracture corresponds to newly formed ice that has frozen in the lead as frazil and then been herded to the lead edge by wind or currents where it accumulates as slush. (*b*) Six hours later, the lead is approximately 3 times as wide. A narrow band of open water occurs along the upper edge of the fracture (sinuous, light gray feature). Most of the lead has frozen in new ice (dark area).

4. Old fractures tend to be radiometrically warmer than new fractures for reasons that are not fully understood.

5. The probability of detecting a feature increases with its age.

6. New fractures are the least likely features to be detected.

7. Feature signatures recorded by scanning passive microwave sensors are independent of the orientation of the ridge or fracture as measured with respect to scan direction of the antenna assembly.

8. The range of contrast values measured for features in different width categories does not decline substantially from that observed for the largest features unless width is less than 10 m or approximately 40% of the passive microwave sensor's 26-m beam diameter.

9. In KRMS data studied here, the presence of snow does not affect radiometric contrast of either fractures or ridges; nor does it alter the range of brightness temperatures observed for fractures. Brightness temperatures of snow-covered ridges, however, extend across a range that is approximately 15 K cooler and 10 K warmer than the range observed for snow-free ridges.

10. Fractures cannot be discriminated from pressure ridges on the basis of brightness temperature, radiometric contrast, or characteristics of radiometric profiles measured across these features.

Data on which these conclusions are based represent ice conditions along a single track through the Beaufort-Chukchi Sea region during mid-March 1983 as imaged at a single frequency and polarization. Imagery obtained in other spectral bands with sensors of higher spatial resolving power may well show enhanced feature characterization capability. General applicability of these results to deformational features that occur across the entire arctic region must be verified by additional work that demonstrates that similar relationships exist elsewhere. In the marginal ice zone and in regions where seasonal ice predominates, such as the Bering, Labrador, Okhotsk, and Baltic seas, deformational features may well assume radiometric characteristics that differ significantly from those reported here, because of generally thinner ice, increased dynamics, greater precipitation, thicker snow cover, and warmer surface physical temperature. Nonetheless, surface studies conducted over the last decade suggest that the radiometric ingredients of conceptual models presented above have at most a weak regional dependence. Throughout much of the Arctic Basin, moreover, where mixtures of multiyear ice and first-year ice prevail, processes that create fractures and pressure ridges and alter their radiometric signatures are not expected to differ markedly from those operative in the restricted region investigated here.

Several issues that concern passive microwave signatures of deformational features remain unresolved. First, improved radiometric models must be developed to explain signatures associated with pressure ridges. Second, time series data are required to document the evolution of ridge and fracture signatures over long periods (months to years). It remains unclear, for example, whether all ridge signatures follow similar evolutionary paths, or whether physical characteristics of newly formed ridges coupled with local environmental parameters lead to several possible outcomes. Finally, work is needed to combine passive microwave signatures, such as those analyzed here, with coincident active microwave signatures obtained with SAR and SLAR sensors. It is clear from this paper and the work of others that neither class of sensors, passive microwave nor active microwave, resolves all deformational features unambiguously. The prospects are good that multisensor analyses which combine the best attributes of each sensor will lead to significant improvements in our ability to map deformational elements of the sea ice pack using remote sensor data.

Acknowledgments. Funds to acquire passive microwave images and aerial photographs analyzed here were provided by the Office of Naval Research (Charles Luther, program manager) and by the Naval Ocean Research and Development Activity under Department of Defense program element 0601153N. Analysis of these data was supported by the Naval Oceanographic and Atmospheric Research Laboratory (NOARL) under Department of Defense program element 0601153N through the Sea Ice Classification project (Herbert Eppert, program manager). We gratefully acknowledge the support of these sponsors. In preparing this manuscript we have drawn extensively from an unpublished report written in the early 1970s by Willy Weeks and Austin Kovacs that describes the mechanics of ridge and fracture formation. Thorough reviews by three anonymous readers proved exceptionally valuable in revising and improving the original manuscript. Drew Urbassik of ESL-TRW Corporation provided technical assistance in use of the IDIMS image processing system. We thank both Gary Maykut of the University of Washington for use of his GMPLOT software, and David Bell of NOARL, who in the absence of GMPLOT documentation skillfully hacked out drafts of scatter plots that appear herein. NOARL contribution JA:332:029:92.

REFERENCES

Assur, A., Breakup of pack ice floes, in *Ice and Snow*, edited by W. D. Kingery, pp. 335–347, MIT Press, Cambridge, Mass., 1963.

Breslau, L. R., J. D. Johnson, J. A. MacIntosh, and L. D. Farmer, The development of arctic sea transportation, *Mar. Technol. Soc. J.*, *4*(5), 19–43, 1970.

Campbell, W. J., P. Gloersen, W. J. Webster, T. T. Wilheit, and R. O. Ramseier, Beaufort Sea ice zones as delineated by microwave imagery, *J. Geophys. Res.*, *81*(6), 1103–1110, 1976.

Campbell, W. J., et al., Microwave remote sensing of sea ice in the AIDJEX Main Experiment, *Boundary Layer Meteorol.*, *13*, 309–337, 1978.

Cavalieri, D. J., J. P. Crawford, M. R. Drinkwater, D. T. Eppler, L. D. Farmer, R. R. Jentz, and C. C. Wackerman, Aircraft active and passive microwave validation of sea ice concentration from the Defense Meteorological Satellite Program special sensor microwave image, *J. Geophys. Res.*, *96*(C12), 21,989–22,008, 1991.

Eppler, D. T., and L. D. Farmer, Texture analysis of radiometric signatures of new ice forming in arctic leads, *IEEE Trans. Geosci. Remote Sens.*, *GE-29*(2), 233–241, 1991.

Eppler, D. T., and B. M. Heydlauff, Digitizing KRMS analog data on a personal computer, *NORDA Rep. 219*, 19 pp., Nav. Oceanogr. and Atmos. Res. Lab., Stennis Space Cent., Miss., 1990.

Eppler, D. T., L. D. Farmer, A. W. Lohanick, and M. Hoover, Classification of sea ice types with single-band (33.6 GHz) airborne passive microwave imagery, *J. Geophys. Res.*, *91*(C9), 10,661–10,695, 1986.

Eppler, D. T., L. D. Farmer, and A. W. Lohanick, On the relationship between ice thickness and 33.6 GHz brightness temperature observed for first-season sea ice, *in Sea Ice Properties and Processes*, edited by S. F. Ackley and W. F. Weeks, *CRREL Monograph 90-1*, pp. 229–232, U.S. Army Cold Reg. Res. and Eng. Lab., Hanover, N. H., 1990.

Eppler, D. T., L. D. Farmer, and D. L. Bell, Validation of total ice concentration retrieved from SSM/I data with the Navy algorithm, NOARL report, Nav. Oceanogr. and Atmos. Res. Lab., Stennis Space Cent., Miss., in press, 1992.

Farmer, L. D., D. T. Eppler, and A. W. Lohanick, Converting digital passive microwave radiances to Kelvin units of brightness temperature, *NORDA Tech. Note 427*, 16 pp., Nav. Oceanogr. and Atmos. Res. Lab., Stennis Space Cent., Miss., 1990.

Fukutomi, T., and K. Kusunoki, On the form and formation of hummocky ice ranges (in Japanese), *Teion Kagaku*, *8*, 59–88, 1951.

Fung, A. K., and M. F. Chen, Emission from an inhomogeneous layer with irregular interfaces, *Radio Sci.*, *16*(3), 289–298, 1981.

Gloersen, P., W. Nordberg, T. J. Schmugge, T. T. Wilheit, and W. J. Campbell, Microwave signatures of first-year and multiyear sea ice, *J. Geophys. Res.*, *78*(18), 3564–3572, 1973.

Gloersen, P., H. J. Zwally, A. T. C. Chang, D. K. Hall, W. J. Campbell, and R. O. Ramseier, Time-dependence of sea-ice concentration and multiyear ice fraction in the Arctic Basin, *Boundary Layer Meteorol.*, *13*, 339–359, 1978.

Grenfell, T. C., Surface-based passive microwave studies of multiyear sea ice, *J. Geophys. Res.*, *97*(C3), 3485–3501, 1992.

Grenfell, T. C., and A. W. Lohanick, Temporal variations of the microwave signatures of sea ice during late spring and early summer near Mould Bay, NWT, *J. Geophys. Res.*, *90*(C3), 5063–5074, 1985.

Grenfell, T. C., D. L. Bell, A. W. Lohanick, C. T. Swift, and K. St. Germain, Multifrequency passive microwave observations of saline ice grown in a tank, in *Proc. Int. Geosci. and Remote Sens. Symp. (IGARSS '88)*, pp. 1687–1690, Inst. of Electr. and Electron. Eng., New York, 1988.

Hall, D. K., Influence of depth hoar on microwave emission from snow in northern Alaska, *Cold Reg. Sci. Technol.*, *13*, 225–231, 1987.

Hall, D. K., J. L. Foster, and A. T. C. Chang, Measurement and modeling of microwave emission from forested snowfields in Michigan, *Nord. Hydrol.*, *13*, 129–138, 1982.

Hall, D. K., A. T. C. Chang, and J. L. Foster, Detection of the depth-hoar layer in the snow-pack of the arctic coastal plain of Alaska, U.S.A., using satellite data, *J. Glaciol.*, *32*(10), 87–94, 1986.

Hanson, A., Description of a thrust of sea ice, *Arct. Alp. Res.*, *12*(1), 101–104, 1980.

Hollinger, J. P., J. L. Pierce, and G. A. Poe, SSM/I instrument evaluation, *IEEE Trans. Geosci. Remote Sens.*, *GE-28*(5), 781–790, 1990.

Ketchum, R. D., and A. W. Lohanick, Passive microwave imagery of sea ice at 33 GHz, *Remote Sens. Environ.*, *9*, 211–223, 1980.

Ketchum, R. D., L. D. Farmer, and J. P. Welsh, K-band radiometric mapping of sea ice, *NORDA Tech. Note 179*, 18 pp., Naval Oceanogr. and Atmos. Res. Lab., Stennis Space Cent., Miss., 1983.

Kong, J. A., R. Shin, J. C. Shuie, and L. Tsang, Theory and experiment for microwave remote sensing of snow packs, *J. Geophys. Res.*, *84*(B10), 5669–5673, 1979.

Leppäranta, M., and T. Thompson, BEPERS-88: Sea ice remote sensing with synthetic aperture radar in the Baltic Sea, *Eos Trans. AGU*, *70*(28), 698–709, 1989.

Livingstone, C. E., K. P. Singh, and L. Gray, Seasonal and regional variations in active/passive microwave signatures of sea ice, *IEEE Trans. Geosci. Remote Sens.*, *GE-25*(2), 159–173, 1987.

Lohanick, A. W., Snow thickness and brightness temperature on multiyear ice, *NORDA Tech. Note 171*, 12 pp., Nav. Oceanogr. and Atmos. Res. Lab., Stennis Space Cent., Miss., 1982.

Lohanick, A. W., Microwave brightness temperatures of laboratory-grown undeformed first-year ice with an evolving snow cover, *J. Geophys. Res.*, in press, 1993.

Lohanick, A. W., and T. C. Grenfell, Variations in brightness temperature over cold first-year sea ice near Tuktoyaktuk, Northwest Territories, *J. Geophys. Res.*, *91*(C4), 5133–5144, 1986.

Troy, B. E., J. P. Hollinger, R. M. Lerner, and M. M. Wisler, Measurement of the microwave properties of sea ice at 90 GHz and lower frequencies, *J. Geophys. Res.*, *86*(C5), 4283–4289, 1981.

Tucker, W. B., T. C. Grenfell, R. G. Onstott, D. K. Perovich, A. J. Gow, R. A. Shuchman, and L. L. Sutherland, Microwave and physical properties of sea ice in the winter marginal ice zone, *J. Geophys. Res.*, *96*(C3), 4573–4587, 1991.

Ulaby, F. T., and W. H. Stiles, The active and passive response to snow parameters, 2, Water equivalent of dry snow, *J. Geophys. Res.*, *85*(C2), 1045–1049, 1980.

Wilheit, T., W. Nordberg, J. Blinn, W. Campbell, and A. Edgerton, Aircraft measurements of microwave emission from arctic sea ice, *Remote Sens. Environ.*, *2*, 129–139, 1972.

World Meteorological Organization (WMO), *WMO Sea Ice Nomenclature*, 147 pp., Secretariat of the World Meteorological Society, Geneva, 1970.

D. T. Eppler and L. D. Farmer, Bronson Hills Associates, P.O. Box 341, Fairlee, VT 05045.

A. W. Lohanick, AWL Research, 9 Memorial Drive, Lebanon, NH 03766.

(Received January 27, 1992;
revised August 13, 1992;
accepted September 28, 1992.)